Collective localized surface plasmons for high performance fluorescence biosensing

Martin Bauch and Jakub Dostalek*

AIT - Austrian Institute of Technology, Muthgasse 11, 1190 Vienna, Austria
jakub.dostalek@ait.ac.at

Abstract: Metallic nanostructures supporting collective localized surface plasmons (cLSPs) are investigated for the amplification of signal in fluorescence biosensors. cLSPs modes are supported by diffractive arrays of metallic nanoparticles that are embedded in a refractive index-symmetrical environment. They exhibit lower damping and thus their excitation is associated with higher field intensity enhancement and narrower resonance than that for regular localized surface plasmons. Through finite difference time domain (FDTD) simulations, we designed a novel cLSP structure that exhibit two resonances overlapping with absorption and emission wavelengths of assumed fluorophore (similar to Cy5 or Alexa Fluor 647). The simulations of surface plasmon-enhanced fluorescence (PEF) took into account the cLSP-driven excitation, directional emission, and mediated quantum yield in realistic sandwich immunoassays that utilize fluorophore-labeled detection antibodies. Achieved results indicate that cLSP-based structures holds potential for extraordinarily high fluorescence intensity enhancement that exceeds a value of 10^3.

OCIS codes: (240.6680) Surface plasmons; (170.6280) Spectroscopy, fluorescence and luminescence; (280.1415) Biological sensing and sensors; (050.6624) Subwavelength structures.

References and links

1. C. Höppener and L. Novotny, "Exploiting the light-metal interaction for biomolecular sensing and imaging," Q. Rev. Biophys. **45**(2), 209–255 (2012).
2. S. Lal, N. K. Grady, J. Kundu, C. S. Levin, J. B. Lassiter, and N. J. Halas, "Tailoring plasmonic substrates for surface enhanced spectroscopies," Chem. Soc. Rev. **37**(5), 898–911 (2008).
3. B. Sharma, R. R. Frontiera, A. I. Henry, E. Ringe, and R. P. Van Duyne, "SERS: Materials, applications, and the future," Mater. Today **15**(1-2), 16–25 (2012).
4. J. Dostálek and W. Knoll, "Biosensors based on surface plasmon-enhanced fluorescence spectroscopy," Biointerphases **3**(3), FD12–FD22 (2008).
5. K. Aslan, J. Huang, G. M. Wilson, and C. D. Geddes, "Metal-enhanced fluorescence-based RNA sensing," J. Am. Chem. Soc. **128**(13), 4206–4207 (2006).
6. Y. Wang, A. Brunsen, U. Jonas, J. Dostálek, and W. Knoll, "Prostate specific antigen biosensor based on long range surface plasmon-enhanced fluorescence spectroscopy and dextran hydrogel binding matrix," Anal. Chem. **81**(23), 9625–9632 (2009).
7. C. J. Huang, J. Dostalek, and W. Knoll, "Long range surface plasmon and hydrogel optical waveguide field-enhanced fluorescence biosensor with 3D hydrogel binding matrix: On the role of diffusion mass transfer," Biosens. Bioelectron. **26**(4), 1425–1431 (2010).
8. L. Touahir, E. Galopin, R. Boukherroub, A. C. Gouget-Laemmel, J. N. Chazalviel, F. Ozanam, and S. Szunerits, "Localized surface plasmon-enhanced fluorescence spectroscopy for highly-sensitive real-time detection of DNA hybridization," Biosens. Bioelectron. **25**(12), 2579–2585 (2010).
9. K. Tawa, H. Hori, K. Kintaka, K. Kiyosue, Y. Tatsu, and J. Nishii, "Optical microscopic observation of fluorescence enhanced by grating-coupled surface plasmon resonance," Opt. Express **16**(13), 9781–9790 (2008).
10. H. Aouani, O. Mahboub, N. Bonod, E. Devaux, E. Popov, H. Rigneault, T. W. Ebbesen, and J. Wenger, "Bright unidirectional fluorescence emission of molecules in a nanoaperture with plasmonic corrugations," Nano Lett. **11**(2), 637–644 (2011).

#191622 - $15.00 USD Received 10 Jun 2013; revised 7 Aug 2013; accepted 13 Aug 2013; published 23 Aug 2013

11. X. Q. Cui, K. Tawa, K. Kintaka, and J. Nishii, "Enhanced fluorescence microscopic imaging by plasmonic nanostructures: From a 1D grating to a 2D nanohole array," Adv. Funct. Mater. **20**(6), 945–950 (2010).
12. A. Kinkhabwala, Z. F. Yu, S. H. Fan, Y. Avlasevich, K. Mullen, and W. E. Moerner, "Large single-molecule fluorescence enhancements produced by a bowtie nanoantenna," Nat. Photonics **3**(11), 654–657 (2009).
13. Y. Z. Chu, E. Schonbrun, T. Yang, and K. B. Crozier, "Experimental observation of narrow surface plasmon resonances in gold nanoparticle arrays," Appl. Phys. Lett. **93**(18), 181108 (2008).
14. B. Lamprecht, G. Schider, R. T. Lechner, H. Ditlbacher, J. R. Krenn, A. Leitner, and F. R. Aussenegg, "Metal nanoparticle gratings: Influence of dipolar particle interaction on the plasmon resonance," Phys. Rev. Lett. **84**(20), 4721–4724 (2000).
15. G. Vecchi, V. Giannini, and J. Gómez Rivas, "Surface modes in plasmonic crystals induced by diffractive coupling of nanoantennas," Phys. Rev. B **80**(20), 201401 (2009).
16. B. Auguié, X. M. Bendaña, W. L. Barnes, and F. J. García de Abajo, "Diffractive arrays of gold nanoparticles near an interface: Critical role of the substrate," Phys. Rev. B **82**(15), 155447 (2010).
17. G. Vecchi, V. Giannini, and J. Gómez Rivas, "Shaping the fluorescent emission by lattice resonances in plasmonic crystals of nanoantennas," Phys. Rev. Lett. **102**(14), 146807 (2009).
18. M. H. Chowdhury, J. Pond, S. K. Gray, and J. R. Lakowicz, "Systematic computational study of the effect of silver nanoparticle dimers on the coupled emission from nearby fluorophores," J. Phys. Chem. C **112**(30), 11236–11249 (2008).
19. P. Bharadwaj and L. Novotny, "Spectral dependence of single molecule fluorescence enhancement," Opt. Express **15**(21), 14266–14274 (2007).
20. M. Slootsky and S. R. Forrest, "Full-wave simulation of enhanced outcoupling of organic light-emitting devices with an embedded low-index grid," Appl. Phys. Lett. **94**(16), 163302 (2009).
21. G. W. Ford and W. H. Weber, "Electromagnetic interactions of molecules with metal surfaces," Phys. Rep. **113**(4), 195–287 (1984).
22. P. B. Johnson and R. W. Christy, "Optical-constants of noble-metals," Phys. Rev. B **6**(12), 4370–4379 (1972).
23. P. Bharadwaj, B. Deutsch, and L. Novotny, "Optical antennas," Adv. Opt. Photon. **1**(3), 438–483 (2009).
24. T. Jøssang, J. Feder, and E. Rosenqvist, "Photon correlation spectroscopy of human IgG," J. Protein Chem. **7**(2), 165–171 (1988).
25. W. Zhou and T. W. Odom, "Tunable subradiant lattice plasmons by out-of-plane dipolar interactions," Nat. Nanotechnol. **6**(7), 423–427 (2011).
26. A. Christ, T. Zentgraf, S. G. Tikhodeev, N. A. Gippius, J. Kuhl, and H. Giessen, "Controlling the interaction between localized and delocalized surface plasmon modes: experiment and numerical calculations," Phys. Rev. B **74**(15), 155435 (2006).
27. N. Papanikolaou, "Optical properties of metallic nanoparticle arrays on a thin metallic film," Phys. Rev. B **75**(23), 235426 (2007).
28. Y. Z. Chu and K. B. Crozier, "Experimental study of the interaction between localized and propagating surface plasmons," Opt. Lett. **34**(3), 244–246 (2009).
29. M. T. Zin, K. Leong, N. Y. Wong, H. Ma, M. Sarikaya, and A. K. Y. Jen, "Surface-plasmon-enhanced fluorescence from periodic quantum dot arrays through distance control using biomolecular linkers," Nanotechnology **20**(1), 015305 (2009).
30. T. Ruckstuhl, M. Rankl, and S. Seeger, "Highly sensitive biosensing using a supercritical angle fluorescence (SAF) instrument," Biosens. Bioelectron. **18**(9), 1193–1199 (2003).
31. T. Ruckstuhl and D. Verdes, "Supercritical angle fluorescence (SAF) microscopy," Opt. Express **12**(18), 4246–4254 (2004).
32. L. Feuz, P. Jönsson, M. P. Jonsson, and F. Höök, "Improving the limit of detection of nanoscale sensors by directed binding to high-sensitivity areas," ACS Nano **4**(4), 2167–2177 (2010).

1. Introduction

Current advancements in medical diagnostics, food control, and security require improved tools for rapid analysis of trace amounts of chemical and biological analytes. Plasmonics represent a branch of photonics research that offers an attractive means for signal amplification in various optical spectroscopies that become established for detection of molecular analytes. In particular, they include surface-enhanced Raman spectroscopy (SERS), surface-enhanced infrared spectroscopy (SEIRA), and surface plasmon-enhanced fluorescence spectroscopy (PEF) [1–4]. Among these, fluorescence is arguably a mostly spread optical technique for detection of molecular analytes. In routinely used fluorescence assays, fluorophores such as organic dyes or quantum dots serve as labels for the detection of analyte capture on a transducer surface with attached molecular recognition elements. In PEF, fluorophore labels are probed with an intense and confined field of surface plasmons – collective oscillation of charge density and associated electromagnetic field on a surface of metallic films or nanoparticles. The interaction with such fields can strongly enhance

#191622 - $15.00 USD Received 10 Jun 2013; revised 7 Aug 2013; accepted 13 Aug 2013; published 23 Aug 2013

fluorescence light intensity and thus allows the analysis of smaller analyte concentrations in a sample. The enhancement due to the surface plasmon-driven excitation and emission at respective wavelengths occurs only in close proximity to a metallic surface. In general, PEF strategies take advantage of the combination of increased excitation rate, directional plasmon-coupled emission, and improved quantum yield.

Up to now, PEF was pursued with structures supporting localized surface plasmons (LSPs) on metallic nanoparticles as well as with surface plasmon polaritons (SPPs) travelling on continuous metallic surfaces. When applied for immunoassay-based analysis of molecular species, PEF allowed reaching limit of detection of as low as femtomolar concentrations [5–7]. Initial studies in PEF (that is also referred as to metal-enhanced fluorescence - MEF) utilized random metallic nanoparticle clusters. Through the excitation of LSPs, the enhancement factor of measured fluorescence intensity *EF* of the order 10^1 was typically observed [8] for commonly used dyes such as Cy5 exhibiting the quantum yield of $\eta^0 \approx 0.3$. The enhancement factor *EF* for similar dyes can be increased to around 10^2 by using metallic structures with better controlled geometries such as relief linear gratings supporting SPPs [9], circular "bulls eye" gratings [10], or two-dimensional silver nanohole arrays [11]. Fluorescence enhancement *EF* is typically measured from an ensemble of dyes which are randomly attached to plasmonic nanostructures on a solid surface. Besides such experiments, studies on individual dye molecules were carried out and showed the highest reported enhancement of $EF = 1.3 \times 10^3$ for specific location and orientation [12]. This large enhancement was observed for a dye with low intrinsic quantum efficiency dye $\eta^0 \approx 0.025$ that was exposed to LSP field confined to 30 nm wide gap between two triangle nanoparticles (so called bowtie nanoantenna). Let us note that narrow gaps between metallic nanoparticles allow for strong confinement and enhancement of the field intensity which makes them excellently suited for *e.g.* SERS. However, a fluorophore at a very close proximity to a metal leads to a strong quenching fluorescence emission due to the Förster energy transfer which reduces the efficiency of PEF.

In this work, we investigate another approach to PEF based on diffractive arrays of metallic nanoparticles supporting collective (lattice) localized surface plasmons (cLSPs). Such structures were reported to exhibit higher field intensity enhancements with respect to individual metallic nanoparticles due to the reduced radiative damping of LSPs modes [13–15]. cLSP can be excited on arrays of metallic nanoparticles suspended in a refractive index symmetrical geometry [16]. In fluorescence spectroscopy, cLSP modes were shown to provide highly directional fluorescence emission measured at a fluorophore emission wavelength λ_{em} [17]. We further investigate cLSP for PEF in more detail by using finite-difference time-domain (FDTD) simulations. In particular, the enhancement through a combination of surface plasmon-driven excitation and emission and surface plasmon-enhanced quantum yield η is studied for realistic sandwich immunoassays with fluorophore labels. Based on these simulations, a novel cLSP two-resonance structure is proposed and shown to hold potential for extraordinary high fluorescence intensity amplification.

2. Methods

Numerical simulations were performed by using FDTD method implemented in a commercially available package FDTD Solutions (Lumerical Solutions Inc., Canada). Arrays of metallic nanoparticles were arranged in a square lattice with a period Λ. The geometry was described by using Cartesian coordinates with $\hat{x}$ and $\hat{y}$ axis lying in the lattice plane and $\hat{z}$ axis perpendicular to lattice plane. Near field electric field intensity $\vec{E}$ (x,y,z) and transmission and reflectivity spectra were calculated by using a unit cell comprising a single metallic nanoparticle with a uniform mesh size of 1 nm and periodic boundary conditions applied in the $\hat{x}$ and $\hat{y}$ direction. Perfectly matched layers were placed below and above the analyzed structure in $\hat{z}$ direction. For the investigation of the surface plasmon-mediated

#191622 - $15.00 USD Received 10 Jun 2013; revised 7 Aug 2013; accepted 13 Aug 2013; published 23 Aug 2013

emission, a fluorophore was represented as an oscillating dipole [18, 19]. In order to calculate the angular distribution of field intensity emitted from an individual dipole, a super-cell comprising arrays with finite number of periods Λ was used similar to other works [20, 21]. A single emitter with defined dipole orientation was placed in the center of the super-cell with PMLs applied to its walls in the plus and minus $\hat{x}$, $\hat{y}$ and $\hat{z}$ directions. The number of periods of the super-cell was adjusted in order to achieve convergence (typically around 40 periods were sufficient). Total emitted power from a dipole P_{em} was calculated by the integration the energy flux through walls of a cube closely surrounding the dipole (cube edge length of 20 nm). Quantum yield of an emitter η that is altered due to the coupling with metallic nanostructures was obtained as a ratio of the energy emitted to the far field P_r and the total emitted energy P_{em}. The energy emitted to far-field was simulated by using a two dimensional detector placed in the plane above and below the nanoparticle arrays. Near-field components of the electric and magnetic field intensity were recorded and transformed into the far-field dependence of P_r on the polar θ and azimuthal φ angles. For the simulations with a super-cell, the central nanoparticle with the dipole source was modeled with a mesh size of 2.5 nm, while the rest of the structure was modeled with a mesh size of 5 nm. The wavelength-dependent optical constants of used metals were obtained from [22].

3. Simulation of surface plasmon-coupled fluorescence

Further, we used a classical fluorescence model in which a fluorophore is approximated with oscillating absorption $\vec{\mu}_{ab}$ and emission $\vec{\mu}_{em}$ dipoles. The excitation rate of a fluorophore γ_e that is irradiated by an incident wave at the absorption wavelength λ_{ab} can be expressed as:

$$\gamma_e \propto \left|\vec{E}(\lambda_{ab})\cdot\vec{\mu}_{ab}\right|^2. \tag{1}$$

Let us note that this Eq. (1) holds for small amplitude of electric intensity $|\vec{E}|$ when the excitation rate is far from saturation. After its excitation, the fluorophore can return to its ground state by emitting a photon at a higher wavelength λ_{em} (radiative decay rate γ_r) or without emitting a photon (non-radiative decay rate γ_{nr}). Further, we assume an intrinsic radiative decay rate γ_r^0 and non-radiative decay rate γ_{nr}^0 for an emitter in homogenous aqueous environment with the quantum yield of $\eta_0 = \gamma_r^0/(\gamma_r^0+\gamma_{nr}^0)$. When the emitter is brought in vicinity to a metallic structure, decay rates are altered leading to a change in the quantum efficiency η [12, 19, 23]:

$$\eta = \frac{\gamma_r/\gamma_r^0}{\gamma_r/\gamma_r^0+\gamma_{abs}/\gamma_r^0+\left(1-\eta^0\right)/\eta^0}. \tag{2}$$

In Eq. (2), the term γ_r/γ_r^0 states for the normalized radiative decay rate and γ_{abs}/γ_r^0 for additional non-radiative decay rate associated with the absorption by the metal. These ratios can be obtained from FDTD simulations as $\gamma_{abs}/\gamma_r^0 = P_r/P_r^0$ and $\gamma_{abs}/\gamma_r^0 = (P_{em}-P_r)/P_r^0$ [12, 18], where P_r^0 is the power radiated to far field by identical dipole in homogenous dielectric medium.

The directionality of surface plasmon-coupled emission was taken into account by using a parameter named collection efficiency *CE*. We assume that only light emitted at λ_{em} into a range of polar angles $\theta = 0-\theta_{\max}$ can contribute to a measurable signal in a realistic biosensor system (*e.g.*, fluorescence light is collected by a lens with a numerical aperture $NA = \sin[\theta_{\max}]$). As following Eq. (3) shows, the *CE* is defined as the emitted power that can

#191622 - $15.00 USD Received 10 Jun 2013; revised 7 Aug 2013; accepted 13 Aug 2013; published 23 Aug 2013

be collected within assumed range of polar angles which is normalized to the total power emitted to the far field:

$$CE = \int_0^{2\pi}\int_0^{\theta_{\max}} P_r(\theta,\varphi)\sin\theta d\varphi d\theta \Big/ \int_0^{2\pi}\int_0^{\pi} P_r(\theta,\varphi)\sin\theta d\varphi d\theta. \qquad (3)$$

Let us note that the enhancement of fluorescence intensity *EF* emitted to a desired spatial angle can be expressed as a product of the contributions due to plasmon-mediated excitation rate, quantum yield, and collection efficiency. Further, this parameter was calculated for an ensemble of fluorophores with random orientation of their emission $\vec{\mu}_{em}$ and absorption $\vec{\mu}_{ab}$ dipoles and arbitrary location on metallic nanoparticle surface as:

$$EF = \frac{\langle \gamma_e \times \eta \times CE \rangle}{\langle \gamma_e^0 \times \eta^0 \times CE^0 \rangle}. \qquad (4)$$

In Eq. (4), the parentheses $\langle\ \rangle$ denote the averaging of fluorescence intensity over different locations and orientations of dipoles and CE^0 states for the collection efficiency for a randomly oriented dipole in homogenous aqueous environment. As Fig. 1 illustrates, two dipole orientations were investigated. In the first case the absorption and emission dipoles are parallel $\vec{\mu}_{ab} \parallel \vec{\mu}_{em}$ which represents a situation where the emitter is static (*e.g.*, the fluorophore is attached to a surface and rotates slowly with respect to $1/[\gamma_r + \gamma_{nr}]$). The other situation applies for rapidly moving fluorophores in which the emission dipole orientation $\vec{\mu}_{em}$ is independent from that of the absorption dipole $\vec{\mu}_{ab}$.

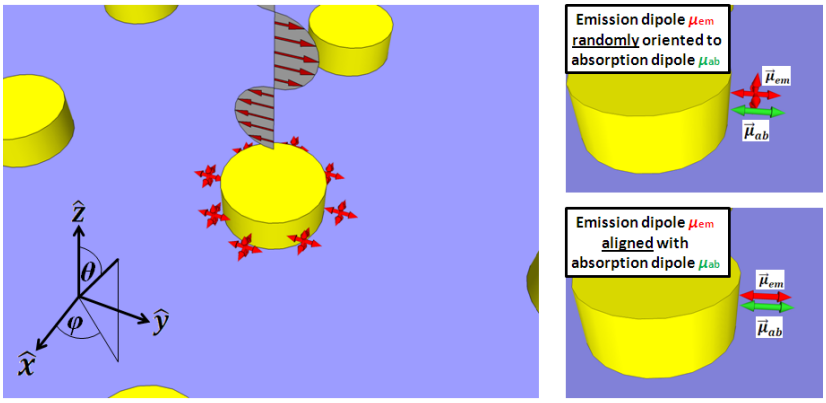

Fig. 1. Schematic of arrays of cylindrical metallic nanoparticles decorated with randomly oriented dipoles representing fluorophores (left) with two possible relations in the orientation of the absorption $\vec{\mu}_{ab}$ and emission $\vec{\mu}_{em}$, dipoles (right).

4. Investigated geometries

The structure that is investigated for the high performance PEF is shown in Fig. 2(a). It consists of a square lattice of gold cylindrical nanoparticles with a diameter D = 110 nm, height h = 50 nm, and a period Λ = 460 nm. These nanoparticles are placed on a surface of a dielectric buffer layer with a low refractive index n_b and a thickness d_b = 120 nm. This buffer layer is on the top of BK7 glass substrate with an optically thick silver film. The whole structure is in contact with an aqueous sample on its top exhibiting a refractive index of n_s = 1.33. Let us note that the buffer layer can be assumed to be made of fluoropolymer materials such as Teflon AF (n_b = 1.32) or Cytop (n_b = 1.34) in order to ensure a refractive index

#191622 - $15.00 USD Received 10 Jun 2013; revised 7 Aug 2013; accepted 13 Aug 2013; published 23 Aug 2013

symmetry. As discussed later, this feature is important for efficient diffraction coupling between metallic nanoparticles leading to the appearance of cLSP modes. As Fig. 2(b) shows, dense arrays (period of Λ = 200 nm) of identical nanoparticles that are placed directly on a BK7 glass surface were used as a reference structure. In addition, a flat BK7 glass surface with and without optically thick gold film was assumed, see Figs. 2(c) and 2(d).

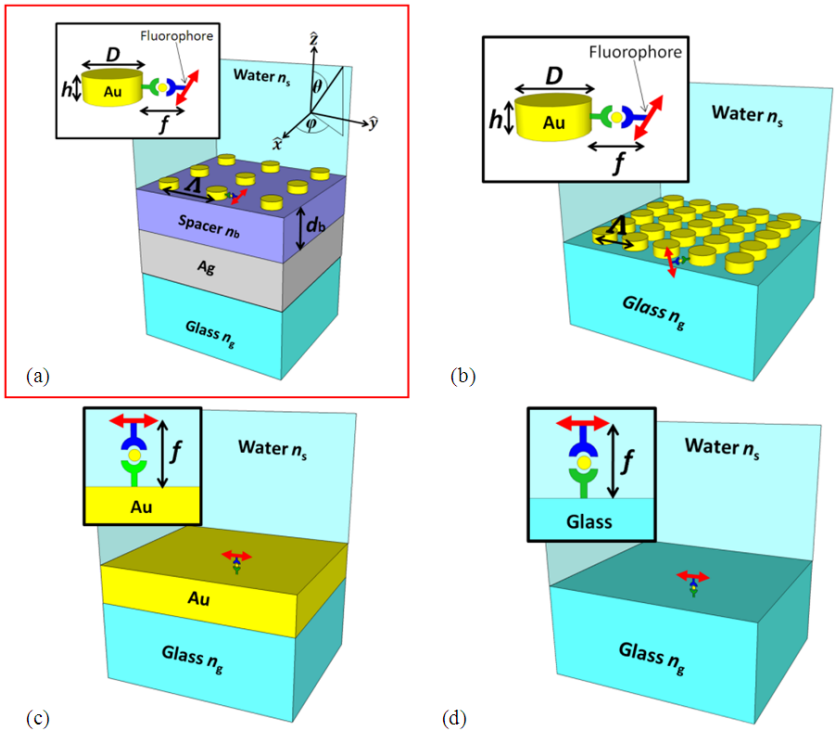

Fig. 2. (a) Schematic of cLSPs-supporting structure and reference structures including (b) dense nanoparticle array on glass substrate, (c) flat gold surface, and (d) flat glass surface. Insets show a model immunoassay with capture antibody (green molecule), captured analyte (yellow molecule), and detection antibody (blue molecule) labeled with a fluorophore (red arrow).

Insets in Fig. 2 illustrate how the investigated structures serve as a solid support for sandwich immunoassay. In this analytical method, a capture antibody (green molecule) is immobilized to a surface and brought in contact with analyzed sample in order to bind a target analyte (yellow molecule). Then, additional detection antibody (blue molecule) that is labeled with a fluorophore (red arrow) is bound to the captured analyte. Afterwards, fluorescence signal emitted by the label is measured and its intensity is related to the amount of analyte present in a sample. The distance between the surface and fluorophore label f is typically above 10 nm and depends on used linker layers and on the size and orientation of antibody and analyte molecules (let us note that typical immunoglobulin G antibody exhibit size around 5 nm [24]). The fluorophore label was assumed to absorb and emit light close to wavelength λ_{ab} = 632.8 nm and λ_{em} = 670 nm, respectively. The intrinsic quantum yield of the fluorophore was varied from η^0 = 1 (ideal emitter), 0.3 (close to that of high quantum yield dyes such as Cy5 and Alexa Fluor 647), and 0.03 (low quantum yield dye). For the nanoparticle arrays, emitters were assumed to be randomly attached around a wall of cylindrical nanoparticles at a distance f, see Figs. 2(a) and 2(b). In addition, f denotes the distance perpendicular to the surface from reference flat surfaces as seen in Figs. 2(c) and 2(d).

#191622 - $15.00 USD Received 10 Jun 2013; revised 7 Aug 2013; accepted 13 Aug 2013; published 23 Aug 2013

5. Results and discussion

5.1 Spectrum of supported modes for investigated structures

Firstly, far field and near field optical properties of cLSP-supporting diffractive arrays of metallic nanoparticles [shown in Fig. 2(a)] are investigated. Figure 3(a) shows a wavelength dependence of the reflectivity calculated for a normally incident plane wave with the electric intensity vector $\vec{E}_0$ parallel to the lattice vector. One can see that the structure was tuned to exhibit two resonances close to the wavelengths λ_{ab} and λ_{em} of assumed fluorophore. These resonances are manifested as narrow dips in the reflectivity spectrum and provide strong enhancement of the electric field intensity $|E/E_0|^2$. The electric field intensity enhancement $|E/E_0|^2$ was calculated at a point located at the distance of f = 20 nm from the metallic nanoparticle wall ($|E/E_0|^2$ averaged over the circumference of a cylindrical disk reaches approximately half of the presented values).

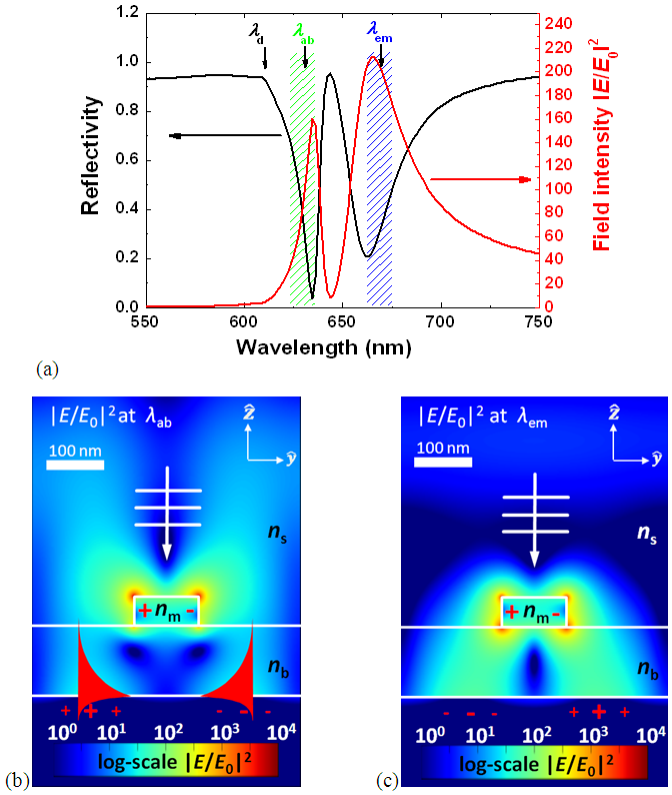

Fig. 3. (a) Wavelength spectrum of reflectivity and electric field intensity enhancement $|E/E_0|^2$ for diffractive arrays of metallic nanoparticles. $|E/E_0|^2$ was calculated for a single point with distance f = 20 nm parallel to $\vec{E}_0$. Detail of spatial distribution of $|E/E_0|^2$ at (b) λ_{ab} and (c) λ_{em} with indicated $\vec{E}_0$ polarization.

In order to elucidate the origin of the two observed resonances at λ_{ab} and λ_{em}, a cross-section of the near-field electric intensity in the *yz* plane was calculated. Results presented in Figs. 3(b) and 3(c) reveal that both resonances are associated with the excitation of LSP mode at gold disk nanoparticles with a dipole moment parallel to the lattice plane. In addition, one can see that the resonances are accompanied with extraordinarily high field intensity enhancement $|E/E_0|^2$ reaching 10^3 at a distance of several nanometers from the nanoparticle surface. This effect is associated with diffraction coupling of LSP modes on neighboring

#191622 - $15.00 USD Received 10 Jun 2013; revised 7 Aug 2013; accepted 13 Aug 2013; published 23 Aug 2013

nanoparticles which leads to the establishing of collective (lattice) localized surface plasmon modes (cLSPs). The excitation of cLSPs is typically manifested as a spectrally narrow resonance which is confirmed in Fig. 3(a) showing, for example for the λ_{ab}, the resonance widths of 25 nm. The origin of this feature lays in the phase-matching of LSPs at wavelengths close to $\lambda_d = \Lambda n_{s,b}$ which results in more efficient trapping of light at the surface, decreased radiative damping, and consequently to increased field enhancement [13–15, 25]. Let us note that this effect is particularly strong when refractive indices of the dielectric above and below the metallic nanoparticle arrays are similar $n_s \sim n_b$.

As seen in Figs. 3(b) and 3(c), the cLSP mode couples to SPPs at the flat silver surface which leads to the split of the resonance. For the (anti-symmetrical) resonance at λ_{em}, charge density oscillations on a flat silver surface exhibit opposite phase with respect to those on the nanoparticle (similarly to mirror charges [26]). This leads to the stronger confinement of the field intensity between the disks and the silver surface. The second (symmetrical) resonance at λ_{ab} is accompanied with the charge density oscillations that are in phase on the silver surface and on the metallic nanoparticles. This mode exhibits an electric intensity field that is more confined in the water medium.

Let us note that when the silver layer is replaced by an infinite buffer layer with $n_s \sim n_b$, the resonance at the wavelength λ_{em} is negligibly changed and the one at λ_{ab} disappears (data not shown). In addition, the resonance at λ_{ab} is close to the wavelength at which SPPs are diffraction excited *via* (0,1) and (1,0) orders on a silver surface. This wavelength can we calculated as [27]:

$$\lambda = \frac{\Lambda}{\sqrt{i^2 + j^2}} \times \mathrm{Re}\left\{ \sqrt{\frac{n_b^2 n_m^2}{n_b^2 + n_m^2}} \right\}, \tag{5}$$

where indices i and j denote diffraction orders. The SPP resonance wavelength of 644 nm is only slightly shifted due to the anti-crossing of SPP dispersion with cLSP resonance (as observed in previous work [28]). The excitation of both modes at λ_{em} and λ_{ab} is strongly sensitive to variations in the thickness of the buffer layer d_b due to the interference with the light back-reflected from the flat silver surface (data not shown).

For comparison, similar data were calculated for three reference geometries depicted in Fig. 2. Dense arrays of gold cylindrical nanoparticles on a glass surface that support regular LSPs [depicted in Fig. 2(b)] represent a geometry that was frequently explored for PEF. For instance, similar arrays with a period of Λ = 200 nm, disk diameter of D = 110 nm, and height of h = 50 nm were used for the amplification of fluorescence signal in the red part of spectrum [29]. As Fig. 4(a) shows, they exhibit much broader resonance that overlaps with λ_{ab} and λ_{em}. In addition, the coupling to the dipolar LSP mode [see Fig. 4(b)] is accompanied with field intensity enhancement ($|E/E_0|^2 \sim 6$ at f = 20 nm) which is more than 30 times smaller than that for the diffractive arrays [see Fig. 3(c)]. Figures 4(c)-4(f) show reflectivity and the electric field intensity distribution on a flat metal and BK7 glass surfaces irradiated by a plane optical wave. Naturally, no plasmonic resonance occurs on these structures and thus no significant field intensity enhancement can be seen. For the gold surface, the field intensity oscillates between $|E/E_0|^2 = 0$ and 4 due to the interference between the incident and back-reflected waves. The enhancement reaches $|E/E_0|^2 = 1.36$ at λ_{ab} = 633 nm at a distance of f = 20 nm which is higher than $|E/E_0|^2 = 0.9$ for the glass surface.

#191622 - $15.00 USD Received 10 Jun 2013; revised 7 Aug 2013; accepted 13 Aug 2013; published 23 Aug 2013

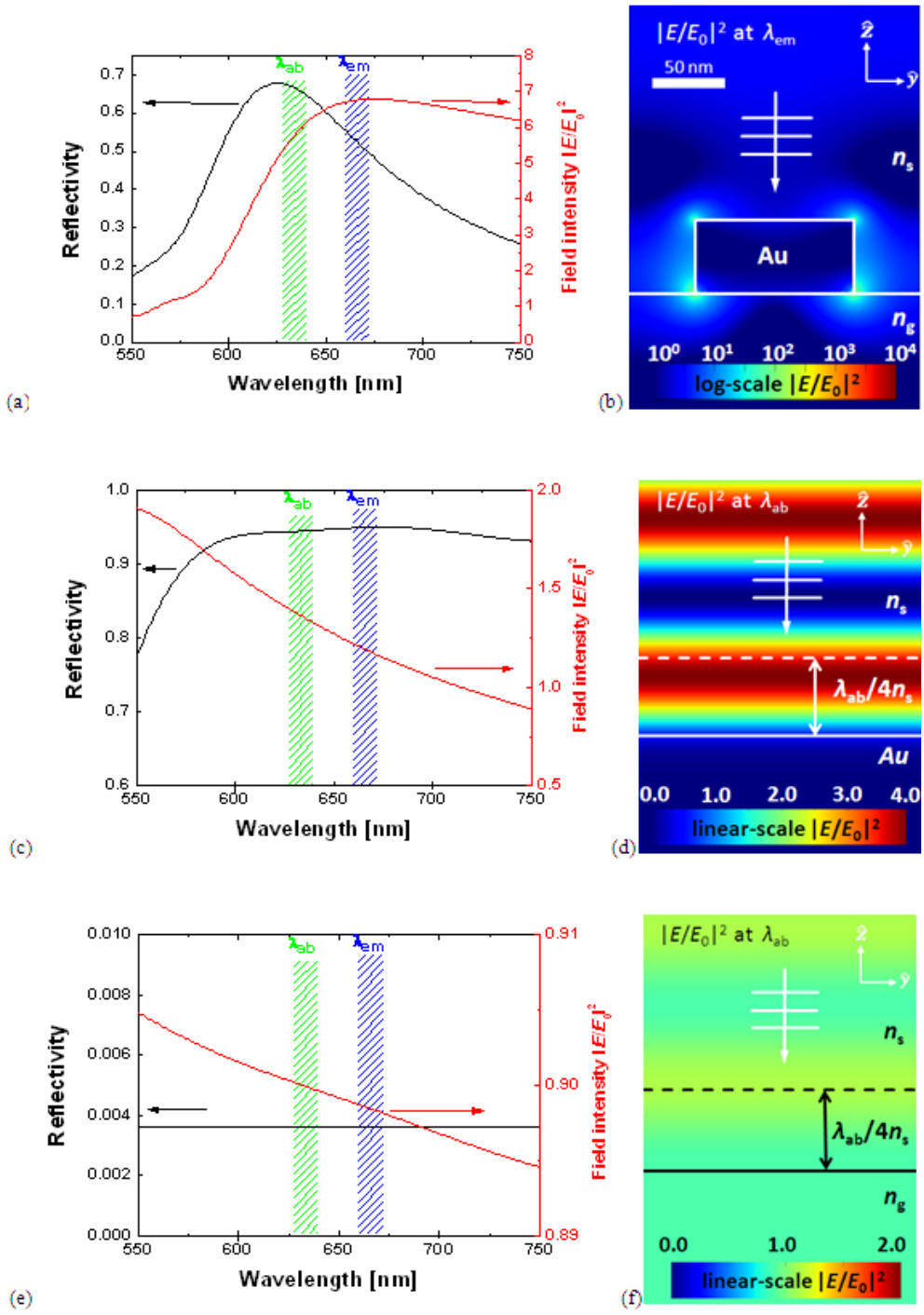

Fig. 4. Reflectivity spectra and electric field intensity enhancement at the distance of $f = 20$ nm for the dense nanoparticle arrays (a-b), flat gold surface (c-d), and BK7 glass surface (e-f). Spatial distribution of the electric field intensity is shown at wavelengths of 670 nm for (b) and 633 nm for (d) and (f).

#191622 - $15.00 USD Received 10 Jun 2013; revised 7 Aug 2013; accepted 13 Aug 2013; published 23 Aug 2013

5.2 Plasmon-driven excitation and emission

As introduced in previous section 3, the plasmonic enhancement of fluorescence intensity can be decomposed to contributions due to the increased excitation rate γ_e at λ_{ab}, directional emission at λ_{em}, and improved quantum yield η. In this section, the interplay of these contributions is investigated for the target structure supporting two cLSPs resonances at the absorption (excitation) wavelength λ_{ab} and emission wavelength λ_{em} and is compared to that for reference structures depicted in Fig. 3. Firstly, the enhancement of excitation rate γ_e/γ_e^0 was obtained from the calculated electric field intensity strength $|E/E_0|^2$ at λ_{ab} by using Eq. (1). The results in Fig. 5(a) show that γ_e/γ_e^0 peaks at the nanoparticle surface and decreases when increasing the distance f. By calculating the excitation rate for different orientations and locations of the absorption dipole on a nanoparticle wall (see Fig. 1), the averaged enhancement of the excitation rate of $\left\langle \gamma_e / \gamma_e^0 \right\rangle = 90$ is predicted at the distance of $f = 20$ nm. This value is order of magnitude higher than that for reference geometries with an emitter located at the same distance f: $\left\langle \gamma_e / \gamma_e^0 \right\rangle = 2.6$ for the dense nanoparticle arrays [Fig. 2(b)], $\left\langle \gamma_e / \gamma_e^0 \right\rangle = 1.36$ for a flat gold surface [Fig. 2(c)], and $\left\langle \gamma_e / \gamma_e^0 \right\rangle = 0.9$ for the BK7 glass surface [Fig. 2(d)].

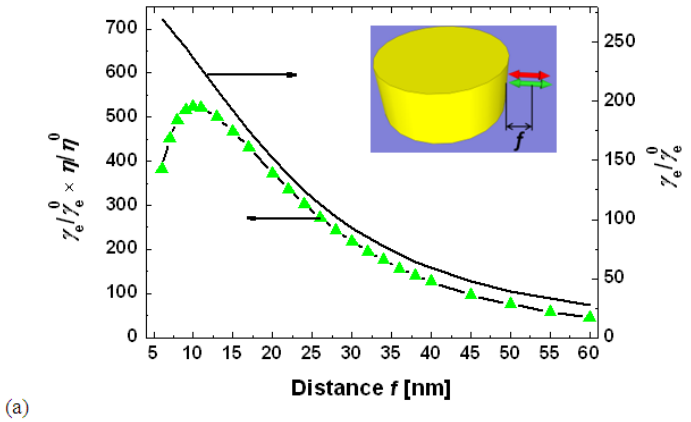

(a)

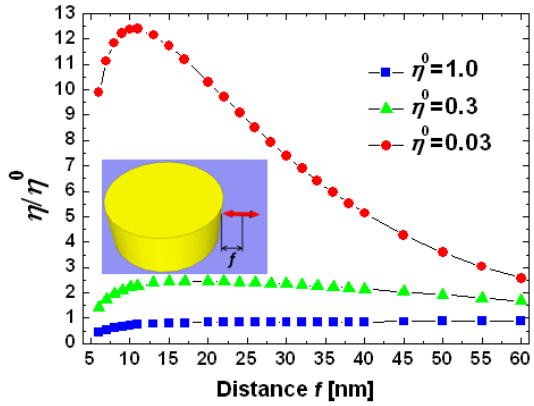

(b)

Fig. 5. (a) Example of the dependence of emission and excitation rates for the cLSP – supporting structure and a fluorophore with $\eta^0 = 0.3$ (b) Distance dependence of the quantum yield η for the fluorophore intrinsic quantum yield of $\eta^0 = 0.03$, 0.3 and 1. The emission and excitation dipole orientations and locations are indicated in respective insets.

#191622 - $15.00 USD Received 10 Jun 2013; revised 7 Aug 2013; accepted 13 Aug 2013; published 23 Aug 2013

The excited fluorophore returns back to its ground state either by emitting a photon at λ_{em} or non-radiatively without emitting a photon. The probability of these processes is typically quantified by the quantum yield η which is defined in Eq. (2). As seen in Fig. 5(b), the interaction with surface plasmons on metallic nanoparticle strongly alters the quantum yield η through the modified local density of optical states (LDOS). In general, this interaction strongly depends on the distance f and it can significantly improve quantum yield η of emitters exhibiting low intrinsic quantum yield in a homogenous environment η^0. For instance, the cLSP-supporting structure provides maximum 12.5-fold enhancement of η at a distance of f = 10 nm for an emitter with η^0 = 0.03. For emitters with higher η^0 = 0.3, smaller 2.5-fold improvement is obtained. Quantum yield of an ideal emitted with η^0 = 1 is always deteriorated due to the effect of damping in the metal. When decreasing distances f below the 10 nm, the quantum yield η is rapidly decreasing due to Förster energy transfer. When increasing the distance f above 30 nm, the quantum yield converges to η^0 as the fluorophore ceases interacting with the confined LSP field.

The combined effect of the enhanced excitation rate γ_e and quantum yield η peaks at distances between f = 10-20 nm from cLSP-supporting structure, see Fig. 5(a). For randomly oriented fluorophore with the intrinsic quantum yield of η^0 = 0.3, the average enhancement of excitation rate and quantum yield reaches $\langle \gamma_e \eta \rangle / \langle \gamma_e^0 \eta^0 \rangle$ = 173. This factor is more than two orders of magnitude higher than obtained that for reference dense nanoparticles arrays (2.6), planar surface with a gold layer (0.53), and for a glass surface (0.92). Let us note that these factors state for the enhancement of far field emission rate into an arbitrary direction. As described further, cLSP-coupled emission allows confining far field emission into a narrow angular cone. This feature is important as it allows improving yield in collecting these photons and delivering them to a detector in realistic optical devices (defined as collecting efficiency [*CE*] in section 3). As Fig. 6 illustrates, emitted light is near-field coupled to cLSP and subsequently diffracted away from the surface into the far field. The direction at which the light is emitted is perpendicular to the surface at λ_{em} as indicated by the respective resonance observed for the normal propagating light wave in Fig. 3(a). The far-field distribution of the emitted light intensity $P_r(\theta,\varphi)$ in Fig. 6 reveals substantially enhanced fluorescence intensity into a cone with polar angles below θ_{max} = 8.5 deg.

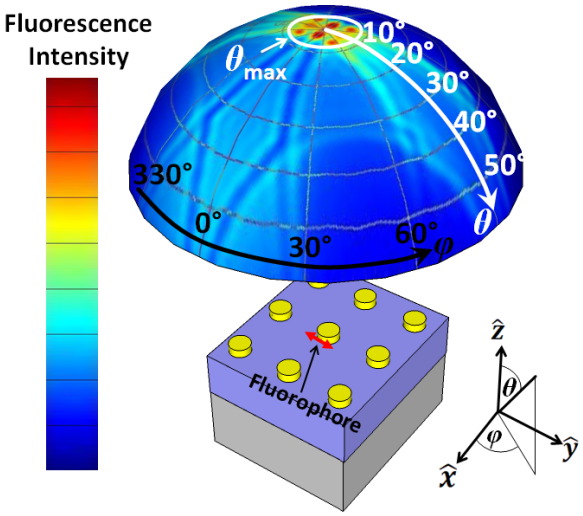

Fig. 6. Example of a far-field emission intensity from a fluorophore on the surface of cLSP-supporting structure. The orientation and position of emission dipole μ_{em} at the distance of f = 20 nm are clearly indicated.

#191622 - $15.00 USD Received 10 Jun 2013; revised 7 Aug 2013; accepted 13 Aug 2013; published 23 Aug 2013

The angular distribution of emitted intensity (such the example presented in Fig. 6) was simulated for different orientations and locations of emitting dipole on the cLSP-supporting and reference structures (see Figs. 1 and 2). From these data, the averaged polar and azimuthal angle dependence of the emitted fluorescence light intensity $\langle P_r(\theta,\varphi)\rangle$ was calculated as presented in Fig. 7. These results allowed us determining the collection efficiency defined by Eq. (3) for the numerical aperture NA = 0.2. Let us note that regular fluorescence microscopes and microarray scanners often uses higher NA. However, the chosen lower NA is expected to allow harnessing directional fluorescence emission and enable decreasing background signal which typically exhibits isotropic angular distribution. For the cLSP-supporting structures, the function $\langle P_r(\theta,\varphi=0)\rangle$ exhibits two narrow lobes at polar angles below θ_{max} = 8.5 deg. This feature and the fact that emitted light does not leak into a glass substrate ensure relatively high collection efficiency CE = 5.2%. On the reference dense arrays of metallic nanoparticles that support regular LSPs, the directionality is not observed and fluorescence light is emitted both towards aqueous sample and into the glass substrate. Therefore, it provides about five times lower collection efficiency of CE = 0.9%. On a flat gold surface, the emission into the substrate is canceled and thus the collection efficiency slightly increases to CE = 1.4%. For emitters at the interface between a glass substrate and water, the majority of fluorescence light is emitted to the substrate in form of supercritical angle fluorescence (SAF) [30, 31]. Compared to this structure, the simulations predict that the proposed cLSP-supporting structure can provide more than 10 times better collection efficiency CE.

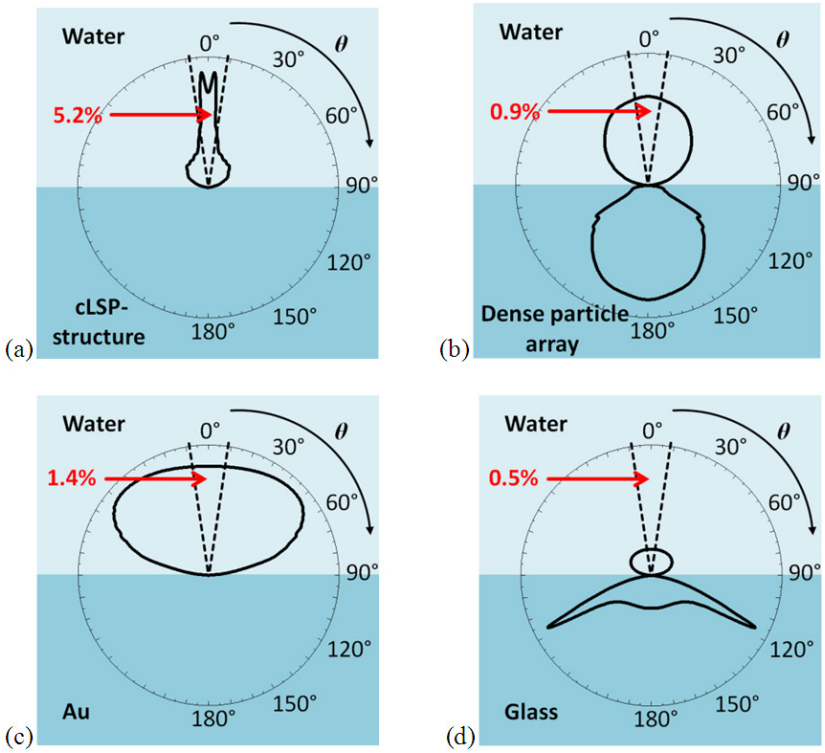

Fig. 7. Comparison of a cross-section of averaged angular fluorescence intensity $<P_r(\theta,\varphi = 0)>$ for (a) cLSP-supporting structure and reference structures including (b) dense nanoparticle particle array supporting regular LSP, (c) flat gold surface, and (d) flat glass surface. Numerical aperture (NA = 0.2) is indicated as a dotted straight line and the calculated collection efficiency CE is clearly shown in each graph.

#191622 - $15.00 USD Received 10 Jun 2013; revised 7 Aug 2013; accepted 13 Aug 2013; published 23 Aug 2013

5.3 Overall performance characteristics

Further, we discuss overall fluorescence enhancement that is associated with the combined effect of the contributions that were separately studied in previous sections 5.1 and 5.2. Let us note that simple product $\langle \gamma_e / \gamma_e^0 \rangle \times \langle \eta / \eta^0 \rangle \times \langle CE / CE^0 \rangle$ does not predict the overall enhancement accurately as the averaging described by the Eq. (4) should be used. Based on that Eq. and above presented results, we simulated the enhancement factor *EF* for fluorophores with an intrinsic quantum yield of η^0 = 0.03, 0.3 and 1. The obtained results are summarized in Fig. 8 for diffractive arrays of metallic nanoparticle as well as for the reference structures. In addition, *EF* was determined for each structure when applied as a substrate for fluorescence measurement with absorption and emission dipoles parallel $\vec{\mu}_{em} \parallel \vec{\mu}_{ab}$ (representing a static fluorophore adhered to a surface) or randomly oriented with respect to each other (representing rapidly rotating fluorophores). The distance from the surface of both dipoles was assumed to be f = 20 nm.

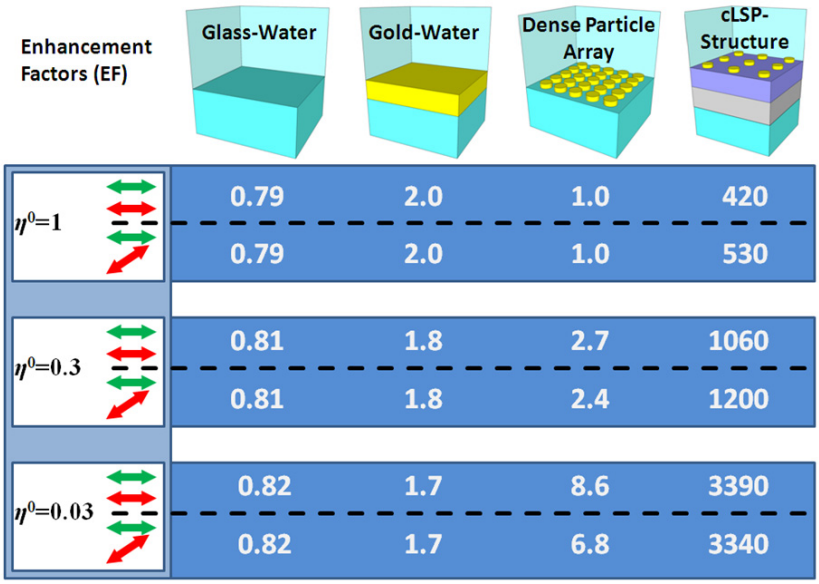

Fig. 8. Summary of the fluorescence intensity enhancement factor *EF* calculated for cLSP-supporting structure (fourth column) compared to a reference structures (first – third column). The data are compared for intrinsic quantum yield of η^0 = 1, 0.3, and 0.03 and two mutual orientations of absorption and emission dipoles.

From the first column in Fig. 8 follows that the fluorescence intensities emitted from an aqueous solution and from a flat glass surface are similar and virtually independent on the intrinsic quantum yield of the fluorophore η^0. For a flat gold surface, the fluorescence intensity emitted to the numerical aperture *NA* = 0.2 is roughly 2.5 times higher than from a glass surface. The main reason is the suppressing of the emission into the substrate [see Fig. 7(c)] and a slightly increased excitation rate [see Fig. 4(c)]. The *EF* on a flat gold surface is weakly decreased for fluorophores with low quantum yield η^0 which is probably due to the effect of the emission *via* SPP modes that does not contribute to the far-field intensity. The data obtained for the non-diffractive (dense) arrays of metallic nanoparticles supporting regular LSPs indicate that only moderate enhancement can be achieved (up to *EF* = 8.6). As reported for other plasmonic structures, the *EF* factor is increasing when decreasing the intrinsic quantum yield η^0. Let us note that the fluorescence enhancement due to the increase of excitation rate [see Fig. 4(b)] is almost compensated by the effect of quenching for

#191622 - $15.00 USD Received 10 Jun 2013; revised 7 Aug 2013; accepted 13 Aug 2013; published 23 Aug 2013

fluorophores with medium and high η^0. In addition, the absence of directivity in the angular distribution of emitted light [see Fig. 7(b)] is impeding the achievement of high *EF*.

The cLSP-supporting structure with diffractive arrays of metallic nanoparticles allows reaching almost three orders of magnitude higher *EF*. The reason is the combined interaction of strong cLSPs field intensity with a fluorophore at both λ_{ab} and λ_{em} (see Fig. 3). Results presented in the fourth column of Fig. 8 summarize that *EF* for fluorophores with η^0~0.3 (such as that of routinely used Cy5 or Alexa Fluor 647) is above 10^3. Even higher enhancement of $EF = 3 \times 10^3$ is predicted for low quantum yield fluorophores with η^0~0.03 which outperforms the best reported PEF enhancement up to now ($EF = 1.3 \times 10^3$ for accurate positioning of a dye with η^0~0.025 [12]). This outstanding performance is in accordance with the partial results showing that the proposed structure provides strongly enhanced excitation rate $|\gamma/\gamma_0|^2 > 10^2$ [see Fig. 3(a)], high directivity that leads to increase in *CE* by a factor >10 [see Fig. 7(a)], and improvement of quantum yield reaching up to 10 for low η^0 [see Fig. 5(b)].

6. Conclusions

The presented work shows that metallic nanoparticles arranged in such a way that they support diffraction-coupled collective localized surface plasmons can provide orders of magnitude stronger plasmonic fluorescence amplification than regular nanoparticle arrays. In particular, the simulations predict that the fluorescence intensity enhancement can exceed 10^3 for a geometry that is compatible with standard sandwich immunoassays utilizing regular chromophores emitting in the red part of spectrum. This outstanding performance is predicted for the structure exhibiting two narrow resonances that overlap with the absorption and emission band of a fluorophore. The simulations took into account plasmon-mediated excitation strength, directional emission, and quantum yield of fluorophore-labeled molecules that attach with random orientation along a wall of metallic cylindrical nanoparticles. These results in conjunction with current advancement in local functionalization of plasmonic hotspots [32] holds potential to dramatically improve performance of fluorescence-based assays. However, let us note that the enhancement was obtained per attached molecule. Therefore, these results cannot be simply extrapolated for the enhancement of the limit of detection when applied to an assay. This performance can be estimated based on other parameters including surface density of catcher antibodies, analyte mass transfer, and affinity reaction constants which is outside the scope of this paper. Our future work focuses at realization of the proposed cLSP-structure by using nanoimprint lithography and their implementation for the amplification of fluorescence signal in protein microarrays.

Acknowledgments

Dr. Paul Müllner and Dr. Roman Bruck from Austrian Institute of Technology in Vienna for help with establishing the FDTD simulations and Prof. Shuzhou Li from Nanyang Technological University in Singapore for fruitful discussions. This work was partially supported by the Austrian NANO Initiative (FFG and BMVIT) through the NILPlasmonics project within the NILAustria cluster (www.NILAustria.at) and Austrian Science Fund (FWF) through the project ACTIPLAS (P 244920-N20).

#191622 - $15.00 USD Received 10 Jun 2013; revised 7 Aug 2013; accepted 13 Aug 2013; published 23 Aug 2013